Elevated temperature microstructure stability of SLM 304L stainless steel

Tarak Amine and Joseph Newkirk

Materials Science and Engineering Department, Missouri University of Science and Technology

Abstract

At elevated temperatures changes in metallurgical structure can be expected for almost any steel or alloy. In stainless steels, the changes can be grain growth, carbide precipitation, ferrite decomposition, or embrittlement. These phenomena can significantly affect the properties of the stainless steel and would potentially change the functionality of the component. Therefore, the impact of elevated temperatures on the microstructure of SLM 304L stainless steel was studied. The work reported here investigates the influence of different aging times at 300C on microstructure and mechanical properties of stainless steels (304L) fabricated with the Selective Laser Melting (SLM) process. Microstructure and mechanical properties were dramatically effected at temperatures much lower than expected when compared to samples of wrought stainless steel. The stainless steel fabricated using the SLM process was more kinetically active than expected based on previous studies of 304L. Results of this study will be presented along with possible reasons for the higher activity.

1. Introduction

Additive manufacturing materials fabricated by the SLM process are used increasingly more in industrial applications due to SLM's ability to fabricate complicated parts geometry coupled with restricted tolerances and the availability of a wide range of alloy compositions. Moreover, austenitic stainless steels are extensively used in a lot of applications where operating temperatures are in the range 290–325 ∘C, such as the nuclear industry for core internal structures and primary recirculation piping. This is due to its superior properties in corrosion resistance, ductility, strength, formability, and weldability [1]. During the cooling process, the primary δ-ferrite solidifies in the melting zone and then the $\delta \rightarrow \gamma$ transformation takes place. Since the $\delta \rightarrow \gamma$ transformation is a diffusion controlled process, the fast cooling rate in the SLM process does not offer sufficient time to complete this phase transformation. As a result, the primary δ-ferrite is retained in the microstructure. However, the ferrite phase is a metastable phase, which transforms to various other embrittling phases at elevated temperature applications [2–5]. Therefore, the ferrite phase may become embrittled after exposure to long term aging at low aging temperatures.

The two ferrite and austenite constituents cannot be equally stable at elevated temperatures. It is anticipated, therefore, that the austenitic stainless steel of the alloys can create the different potential for thermal aging embrittlement in different portions through decomposition of existing phases and/or precipitation of new phases. In this work, low temperature aging behavior of austenitic SS type 304L was studied after aging at 300 ∘C for different aging time up to 1000 hr.

2. Materials and Test Method

In this work, 304L stainless steel powder with particle sizes less than 45 μm were used as the starting material in SLM experiments. The chemical composition of the powder is listed in table 1. A Renishaw AM 250 machine was used to process the 304 stainless steel powder. One sample was investigated in the as-built condition. The other samples were aged at 300 ℃ for different aging time after fabrication (20, 45 minutes, 25, 250, 500, and 1000 hr). The aged samples were packed in heat treating bags, made of type 309 stainless steel, to reduce decarburization and oxidation. Then the samples were cooled in air after the aging process. Once cool, samples were unpacked and prepared for tensile testing.

Table 1:- The chemical composition of 304L stainless steel powder

Element	Cr	Cu	Mn	Ni	O	Si	C	N	P	S	Fe
Wt%	18.5	0.1	1.4	9.9	0.02	0.63	0.015	0.09	0.012	0.004	Balance

The samples were fabricated to miniature test pieces in the shape of a "dogbone" and was designed developed by ABI services LLC. The total sample height was 16 mm. The samples were subsequently sliced to 1.5 mm thickness by using Electrical Discharge Machining (EDM). The kerf loss attributed to the EDM cutting was 0.5 mm. Six (6) samples could be extracted from the total 12 mm height. The samples were numbered 1 through 6, starting with the top surface as shown in Figure 1. All samples were polished sequentially with 400, 600 and 800 grit sandpapers prior to tensile testing.
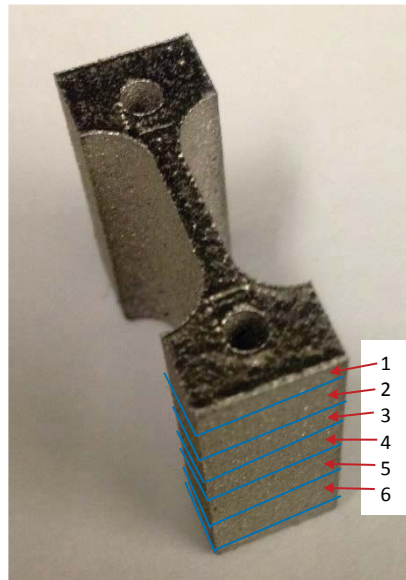

Figure 1: Sliced mini tensile samples of 1.5 mm thickness. Numbers indicate the sample location in term of build height (1 is top of the build, 6 is bottom of the build).

The Automated Ball Indentation (ABI) technique provides a nondestructive and localized alternative to the destructive tensile test [6]. The ABI indentation technique requires a planar spacing of the indents that must be a minimum of three diameters from their centers and be at least two diameters from free edges. The indenter diameter used was 0.03 inch and the load cell used

had a 250 lb capacity. Five ABI measurements were taken on the fabricated blocks of 304L for each of the as-built and aged conditions. Figure 2 shows a micrograph of the general appearance of the indent made in as-built and aged samples using a 0.03 inch diameter indenter from an eight-cycle automated indentation.
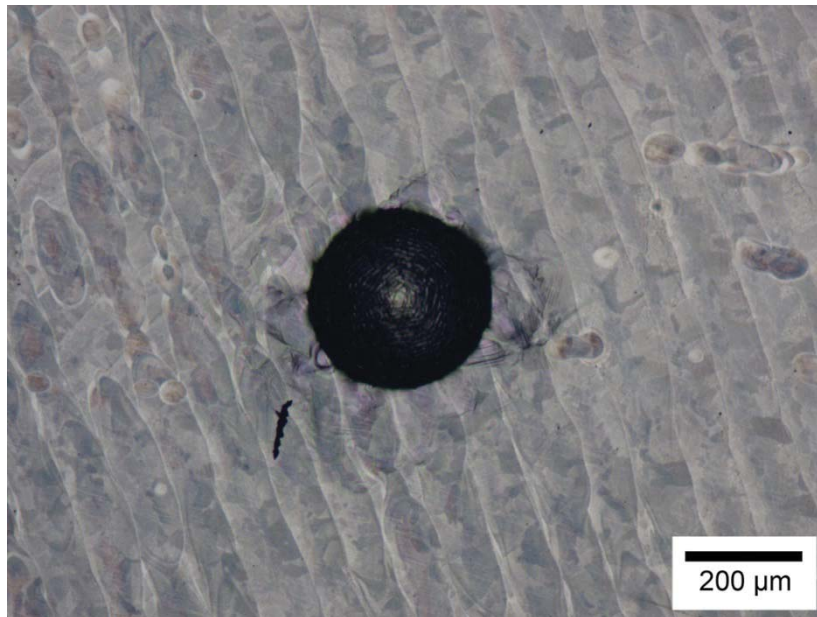

Figure 2: ABI indent in AM304L using a 0.03 inch diameter indenter in as-built material. Note indent covers multiple laser tracks.

Electrolytic etching was used for etching the specimens. The microstructure of the fabricated parts was investigated by optical microscopy. The phase analysis was conducted by X-ray diffraction analysis (XRD) using Philips X Pert-MPD System with Cu Ka radiation and 40 kV and 30 mA operating conditions. Also, initial thermal analysis study has been done by using Differential Scanning Calorimetry (DSC). A microhardness tester equipped with Vickers pyramid indenter was used for microhardness measurements, which were randomly measured on the fabricated samples. A 100 g load was applied by the indenter for 10 seconds.

3.   Results and Discussion

3.1. Microstructure of AM 304L

Figure 3 shows optical micrographs at different locations of the fabricated sample part of as-built material. The sample was etched by electrolytic etching with a solution of 60 percent nitric acid and 40 percent water, and with a relatively low voltage of 1 volt, to delineate the grain boundaries. The optical micrographs indicate that complete melting of the powder occurred. Irregularly shaped pores appeared at various locations. The etching procedure delineated the grain boundaries. The laser tracks, hatching between two neighbor layers, and the different scan strategy

at the fabricated build edges clearly can be seen. The microstructure of as-built 304L material consisted of a mixture of austenite and δ-ferrite as verified by X-ray diffraction.
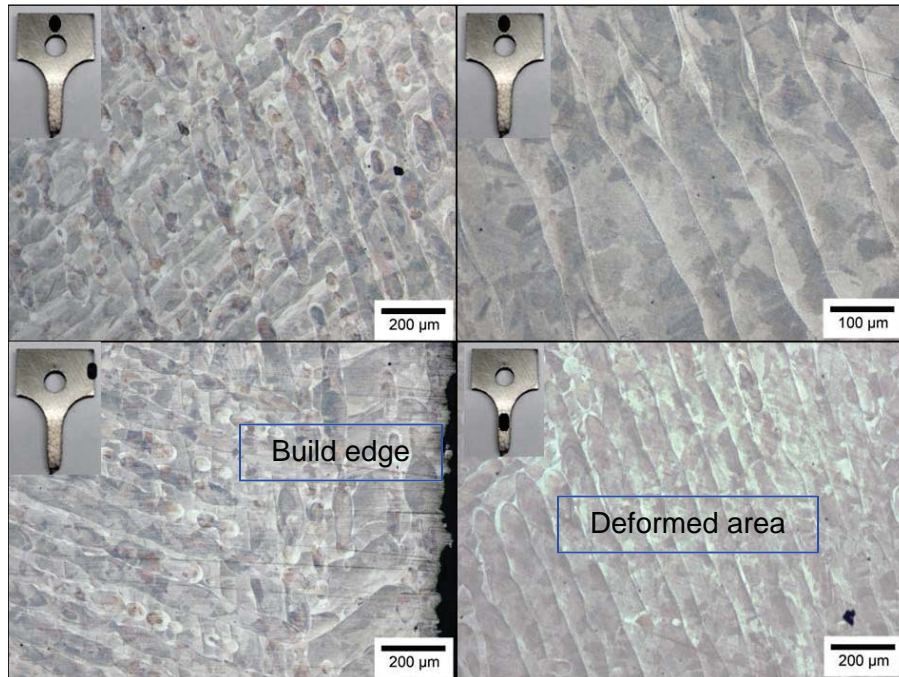

Figure 3: Optical micrographs at different location of As-built material. Locations as marked on broken tensile samples

Figure 4 shows optical micrographs at different locations of the aged samples. The aging temperature was 300 ℃ and the aging time was 250hr and 1000hr. Several pores appeared at the hatch boundaries. The optical micrographs reveal a distinct region in the microstructure on 300 °C aged samples for 250, 500, and 1000 hr at the grain boundaries. This type of structure could be carbide formation ($M_{23}C_6$ or M_2C).
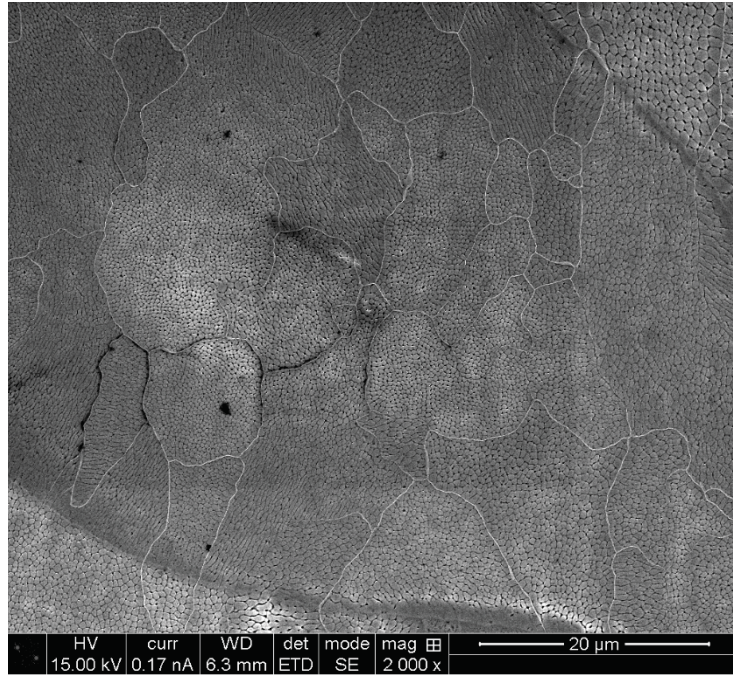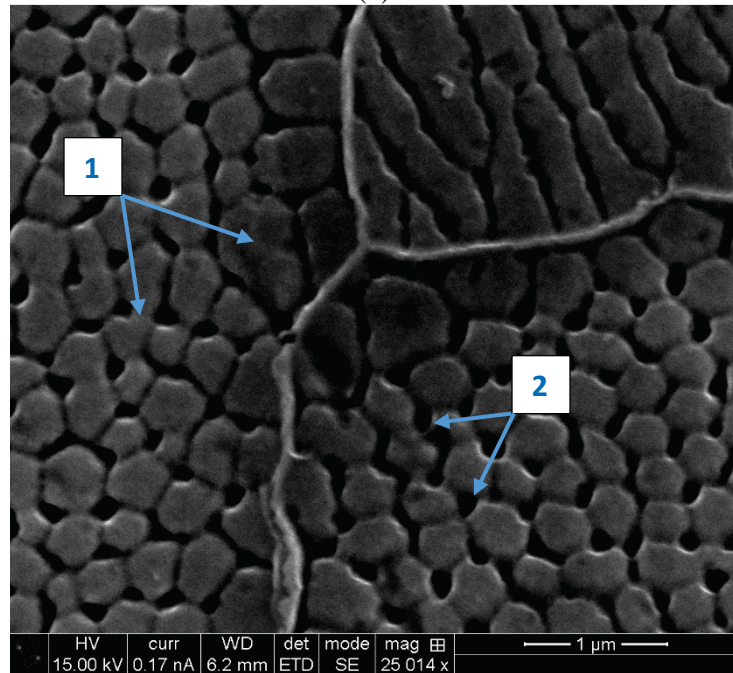
(a)

(b)

Figure 4: Optical micrographs at different location of Aged samples at 300 ℃ for (a) 250hr, (b)1000hr

Figure 5a shows a typical backscatter SEM image of the cellular structure present in the sample. The backscatter mode shown in the higher magnification image in figure 5b reveals two distinct

regions in the microstructure denoted by 1 and 2. Region 1 belongs to the Austenite phase in the cellular structure while region 2 belongs to the δ-ferrite phase.

(a)

(b)

Figure 5:- Typical cellular structure– the SEM micrographs of: (a) the cross-sectional view of the cellular structure, (b) the location of the different phases present in the microstructure.

According to the available literature, while the thermal aging has little effect on the austenite phase, the formation of Cr–rich α' phase by spinodal decomposition of ferrite phase is known to be the primary mechanism for thermal embrittlement [7-11]. This has not been verified here.

During long-term exposure to elevated temperatures of austenitic stainless steels some transformations involving the precipitation of sigma, chi, intermetallic phases, ferrite, and various carbides in addition to change in ferrite / austenite content and alloy recrystallization can take place. These phases are often found at grain boundaries and other high-energy intragranular sites in the form of cubic or needle-like precipitates [12, 13]. These transformations induce remarkable changes in mechanical properties of aged austenitic stainless steels.

According to JMatPro software calculation based on cast parts, these phases cannot be formed at low temperatures, such as 300ºC until years of temperature exposure as shown in figure 6. The JMatPro software assumes a conventional casting cooling rate for the creation of the microstructure, which should be significantly slower than for AM. The JMatPro software calculations were based on 0.1% of amount transformed. The amount transformed must be an amount lower than the amount of phase that exists in equilibrium in order to see the formation of those phases.
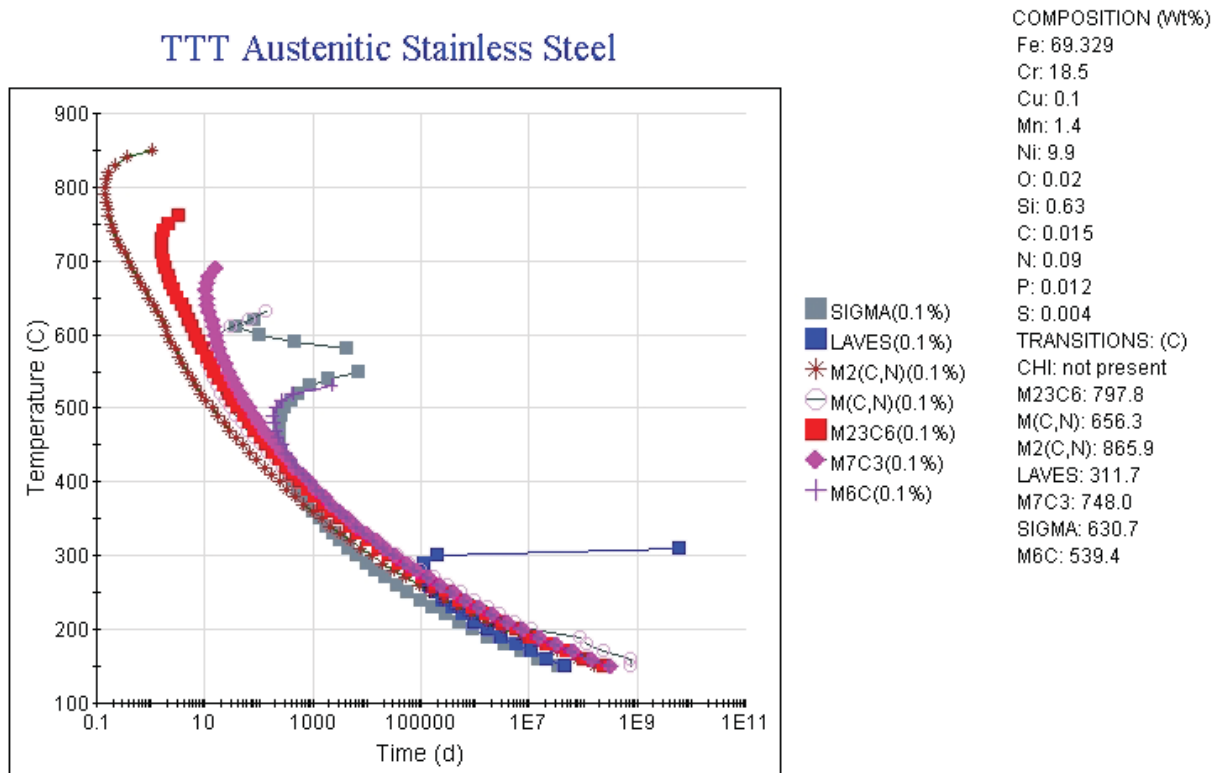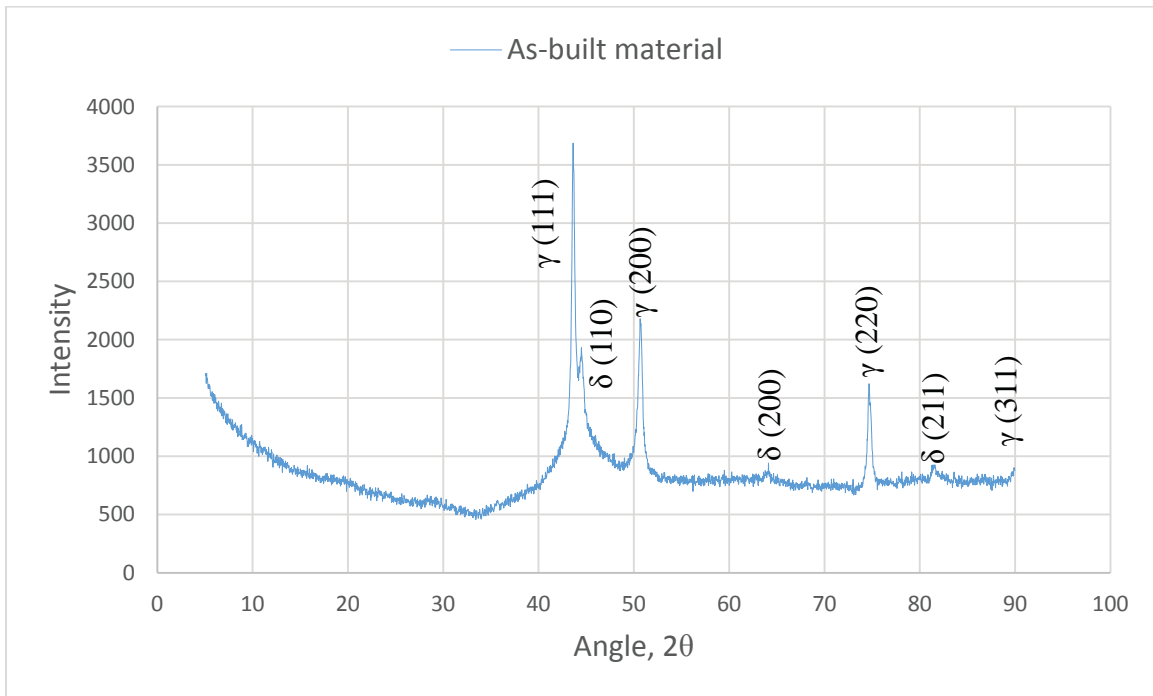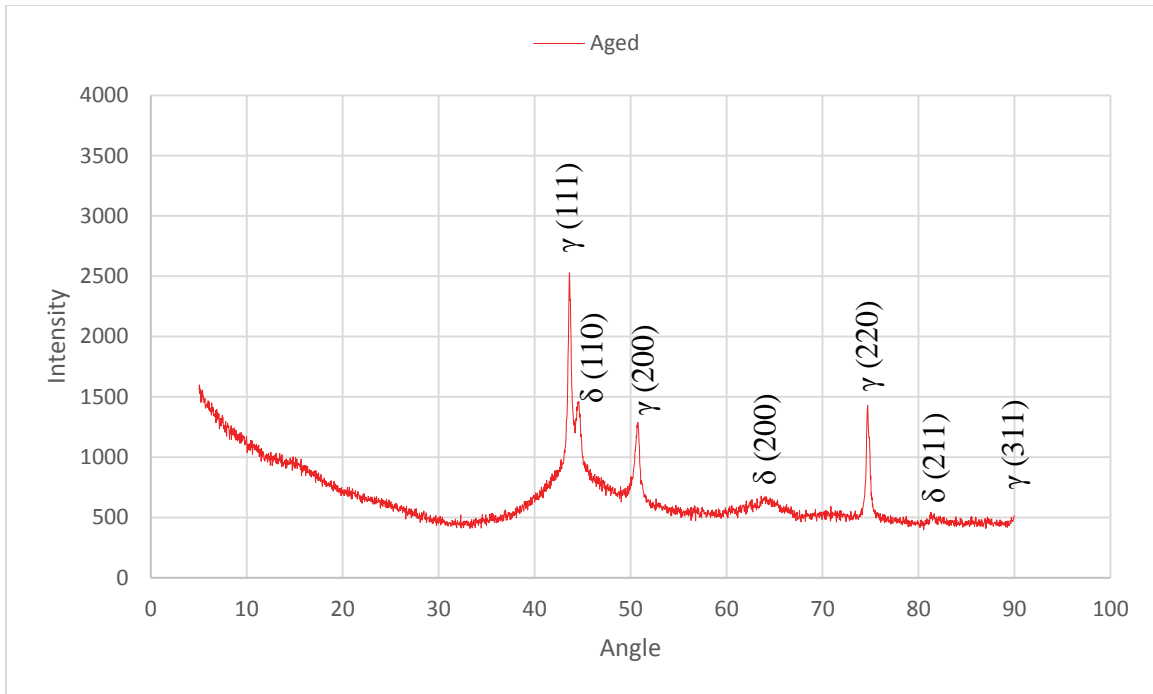

Figure 6: Time - temperature transformation diagram for provided 304L stainless steel powder.

X-ray spectra were produced from the as-built material and aged samples for by scanning 2θ from 0 to 90 degrees, which are shown in figure 7. As can be seen, austenite and δ-ferrite phases were

observed in both as-built and aged samples. The XRD is usually not capable of detecting phases under about 5 vol%. During the cooling process, the primary δ-ferrite solidifies in the melting zone and then the δ→γ transformation takes place. Since the δ→γ transformation is a diffusion controlled process, the fast cooling rate in the selective laser melting process does not offer sufficient time to complete this phase transformation. As a result, the primary δ-ferrite is retained in the microstructure. Determination of the ferrite content is an important issue because of its effects on the hot cracking and joint properties. A small amount of δ-ferrite is considered necessary to avoid the problem of hot cracking during weld solidification. According to the available literature in welding, fully austenitic weld deposits are susceptible to microfissuring during cooling upon solidification [13]. According to the XRD results of ferrite content, it is concluded that the as-built and aged samples are secure against these problems.

(a)

(b)

Figure 7: The XRD spectra of AM 304L stainless steel in (a) As-built material, (b) Aged sample

The DSC technique was used to study the behavior of the material as a function of temperature and time. DSC measures the energy absorbed or released by the sample when it is heated or cooled. The sample was linearly heated twice to 600 ℃ at a heating rate of 10 ℃/min, as shown in figure 8. The DSC curves were not identical for the two runs, demonstrating that the first heated run has a significant effect on the additive material thermal behavior. This could indirectly indicate the magnitude of the energy stored in the as-built material.
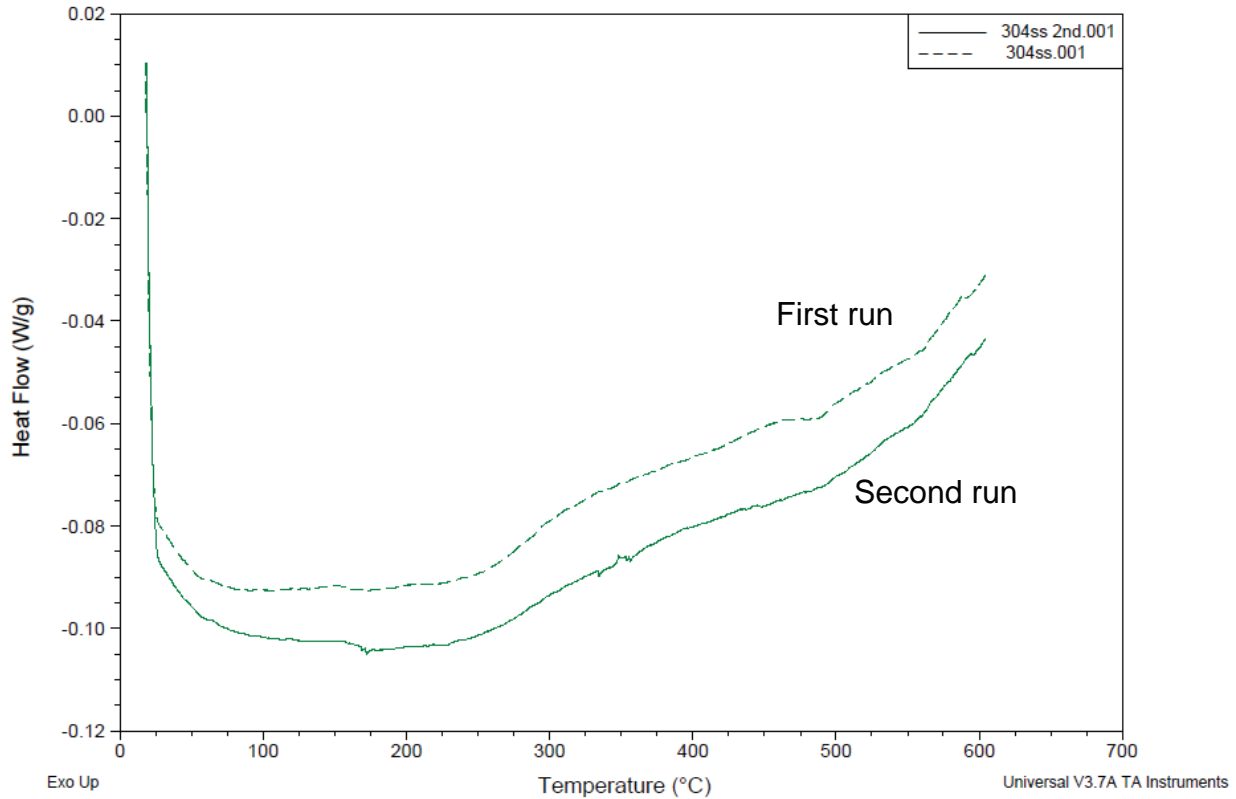
Figure 8:- DSC curve for additive manufactured SS 304L

3.2. Mechanical Properties

Tensile tests of SLM stainless steel 304L was carried out in the as-built and aged conditions. Miniature flat tensile specimens having a cross-section of 1.0 mm × 1.5 mm and a gage length of 8.0 mm. The tensile samples were preloaded with 50 lb and the crosshead velocity was set at 0.0005 in/sec. The load cell used had a 1000 lb capacity.

Figure 9 shows the tensile test results of the as-built material. The results show that the sample from the top of the build is stronger but less ductile compared to the other samples. The other samples have relatively the same strength but slightly different ductility (however, there is no apparent trend in ductility). The sample at the top of the build (sample #1) has the largest strength but the smallest ductility. The top of the build was the last to be melted and did not go through a reheat cycle. Hence it was subjected to the least heat and expected to be harder and less ductile than the other samples from the middle and bottom of the build. The other samples were subjected to more heat, having been reheated because of their location in the build.
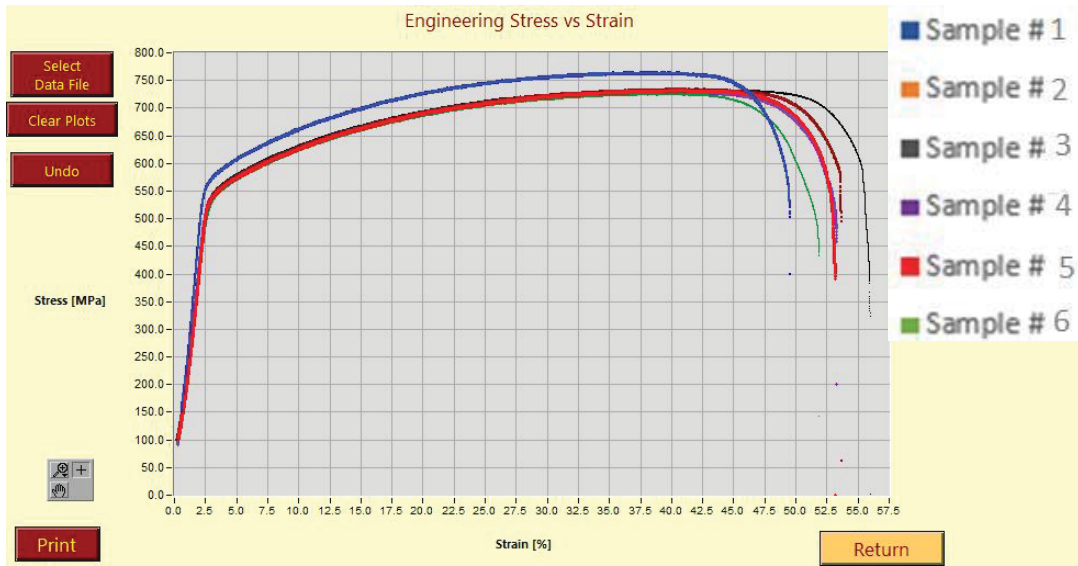
Figure 9: Engineering stress–strain curves of as-built material samples at different reference positions

Figure 10 shows the comparison of the tensile strength of the as-built and aged samples with different aging parameters. The results show that both the yield strength and ultimate tensile strength (UTS) decreased after aging.
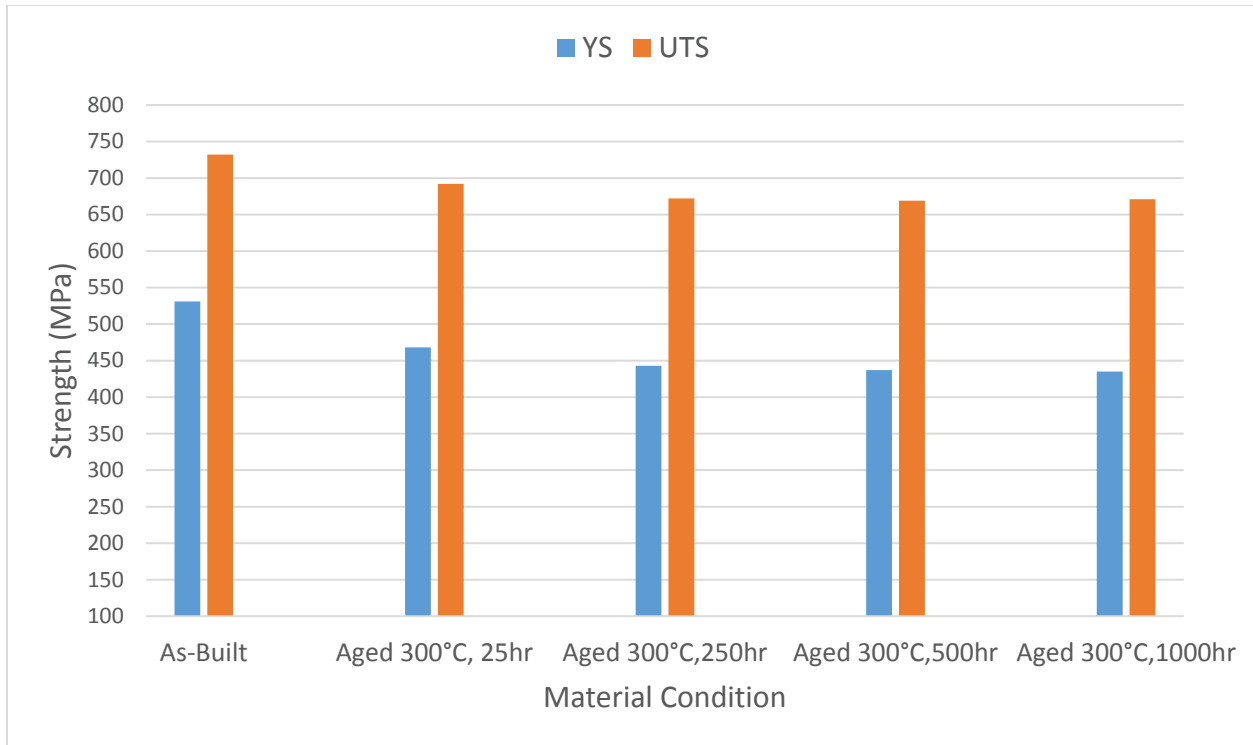
Figure 10: Comparison of tensile strength of the as-built and aged samples with different aging parameters

Figure 11 shows a comparison of tensile strength results from the ABI indentation measurements of the as-built and aged samples at different reference positions. The results show that ultimate tensile strength (UTS) decrease in the aged samples. The ABI results show higher strength values compared to the mini-tensile results. The reason for the difference could be porosity, which the ABI indentation technique is less sensitive to since the ABI test is compressive and multi-axial in nature while the tensile test interrogates a much larger test volume and is an axial (single-axis) test. However, the ABI still shows relatively good agreement with the mini tensile results of yield and ultimate tensile strengths.
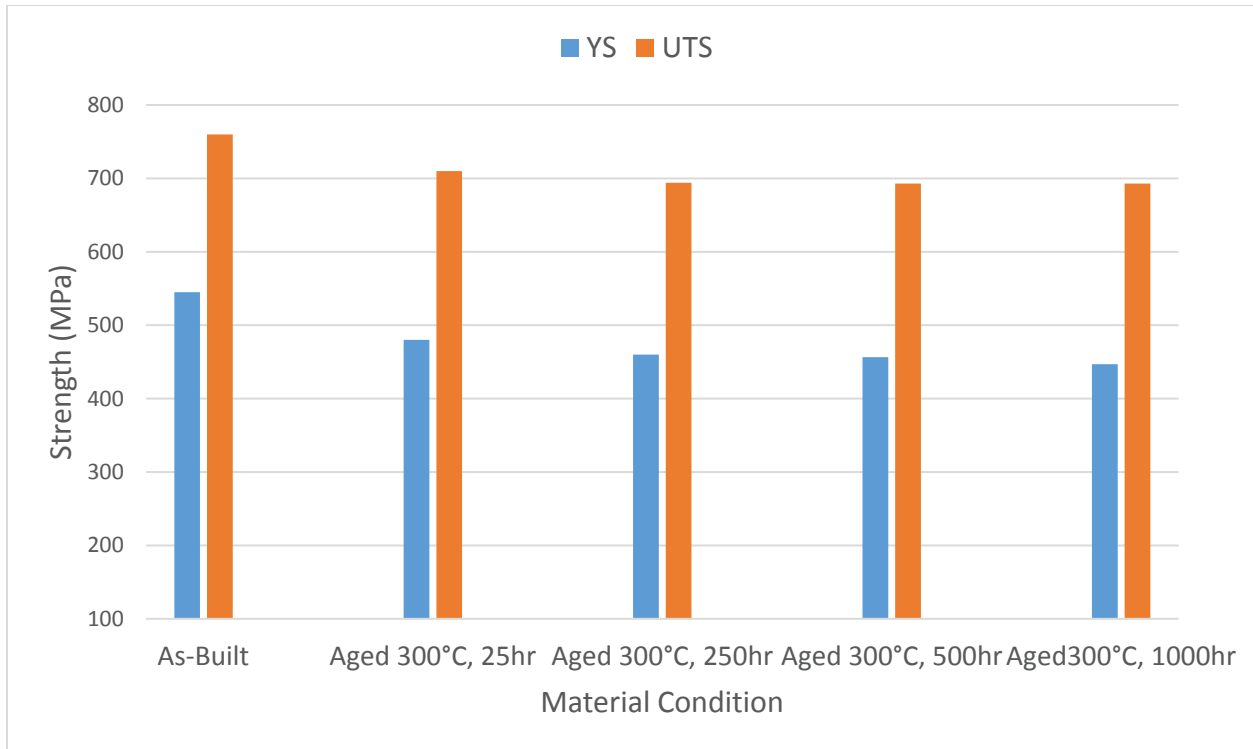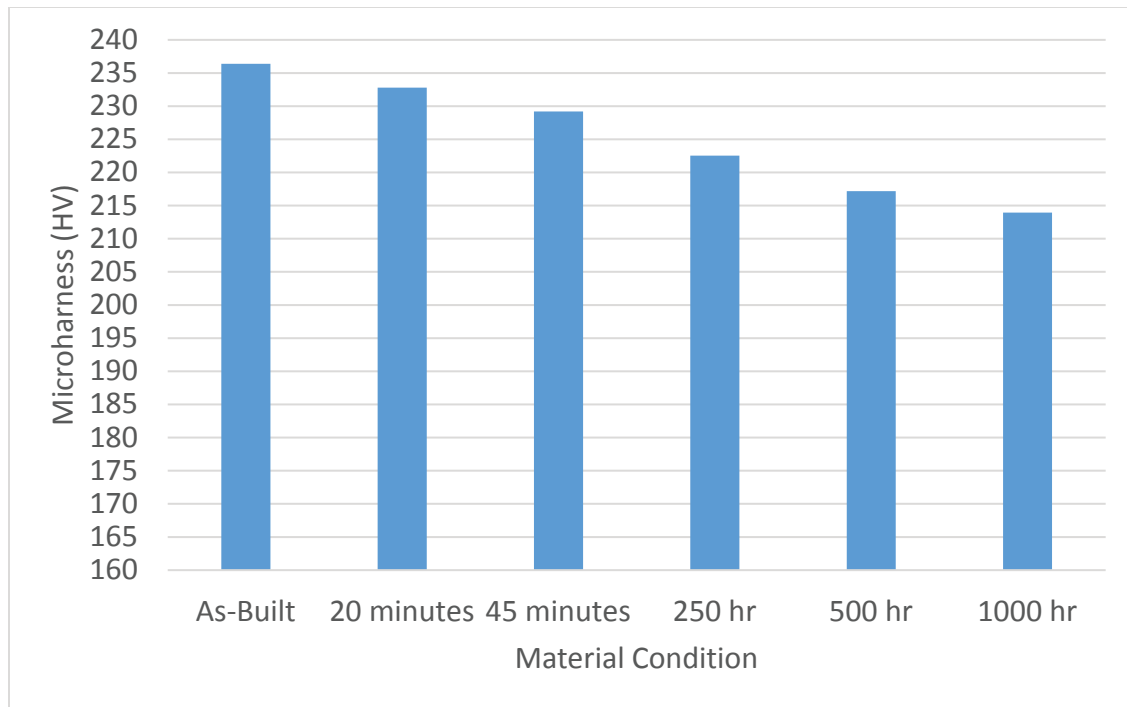
Figure 11: Comparison of tensile strength from ABI measurements of the as-built and aged samples with different aging parameters

The microhardness test results on the as-built and aged samples at 300 ℃ for 20, 45 minutes, and 250, 500, and 1000 hours are shown in figure 12. The load was 981.2 mN and pressing time was 10 secs. The microhardness values shown are the average of ten measurements. Despite some variation in the measured values, a clear trend of continuously decreasing average of the microhardness with increasing aging time was observed. This behavior may be due to the higher δ-ferrite in the as-built material. It is widely known that the presence of δ-ferrite can improve the mechanical strength.

	As-built	Aged 300 °C, 20 minutes	Aged 300 °C, 45 minutes	Aged 300 °C, 250hr	Aged 300 °C, 500 hr	Aged 300 °C, 1000hr
Average	236	233	229	223	217	214
St.d.	7	7	4	7	13	16

Figure 12:- Microhardness measurements of as built and 300 °C aged sample for different aging time

Conclusion

1- For as-built material, a difference in tensile and yield strengths was observed only on the upper surface. The other samples have relatively the same strength and slightly different ductility (there is no apparent trend in ductility).
2- The aged samples have relatively the same strength at each location and slightly different ductility (there is no apparent trend in ductility)
3- Tensile results show that both UTS and YS decreased with increasing aging time.
4- The ABI shows good agreement with the mini tensile results for both the yield and ultimate tensile strengths.
5- The microhardness decreases with increased aging time. This could be due to the decrease in the δ-ferrite content and energy released.
6- The austenite and δ-ferrite phases were observed in both as-built and aged samples.
7- The as-built material appears to have a higher energy stored in the microstructure and is more kinetically active than wrought material of the same composition.

Acknowledgments

References

[1] A.J. Sedricks, Corrosion of Stainless steels, 2nd ed., John Wiley and Sons, New York, NY, 1996, p. 13.

[2] J.M. Vitek, S.A. David, D.J. Alexander, J.R. Keiser, R.K. Nanstad, Acta Metall. 39 (1991) 503–516.

[3] D.J. Alexander, R.K. Nanstad, Proc. of 7th conf. on Environmental Degradation of Materials in Nuclear Power Systems–water reactors, NACE International, Houston, vol. 2, 1995, pp. 747–756.

[4] H. Abe, Y. Watanabe, Metall. Mater. Trans. A 39A (2008) 1392–1398.

[5] W.J. Mills, Int. Mater. Rev. 42 (1997) 45–82.

[6] Haggag, F., Standard Test Methods for: "Nondestructive and Localized Determination of Stress - Strain Curve and Initiation Fracture Toughness of Ferritic Steel Samples and Structures Using Haggag Tensile and Toughness Method (HTTM), 1988 , ABI Services, LLC , Oak Ridge, TN, USA.

[7] Chopra, O. K. and Sather, A., "Initial Assessment of the Mechanisms and Significance of Low–Temperature Embrittlement of Cast Stainless Steels in LWR Systems," Nureg/CR–5385 (ANL–89/17) (1990).

[8] Chung, H. M. and Leax, T. R., "Embrittlement of Laboratory– and Reactor–Aged CF3, CF8, and CF8M Duplex Stainless Steels," Mater. Sci. Technol., 6, 249–262 (1990).

[9] Chung, H.M., "Evaluation of Aging of Cast Stainless Steel Components," ASME Pressure Vessel & Piping Conference, San Diego, CA, June 23-27, (1991).

[10] Chopra, O. K., "Estimation of Fracture Toughness of Cast Stainless Steels during Thermal Aging in LWR Systems, NUREG/CR–4513 (ANL–90/42) (1991).

[11] Michaud, W.F., Toben, P.T., Soppet, W.K., Chopra, O.K., "Tensile-Property Characterization of Thermally Aged Cast Stainless Steels," Nureg/CR-6142 (ANL-93/35) (1994).

[12] Spruiell, J. E., Scott, J. A., Ary, C. S., & Hardin, R. L., "Microstructural stability of thermal-mechanically pretreated type 316 austenitic stainless steel," Metallurgical Transactions, 4(6), 1533-1544 (1973).

[13] K.H. Lo, C.H. Shek, J.K.L. Lai, "Recent developments in stainless steels," Mater Sci Engineer R (65) 39-104 (2009).